EVALUATION OF DYNAMIC COEFFICIENTS FOR FLUID JOURNAL BEARINGS WITH DIFFERENT GEOMETRIES

Tiago Henrique Machado, t046786@dac.unicamp.br
Katia Lucchesi Cavalca, katia@fem.unicamp.br
University of Campinas, Faculty of Mechanical Engineering – Department of Mechanical Design

Abstract. *When two rigid surfaces are in contact and provided with relative motion, their roughness and the stresses shared by both generate friction having positive or negative effects. Regarding the bearings, the friction, which is directly associated with energy dissipation, is considered undesirable. Many studies have dealt with friction reduction procedures. The use of materials to separate the two contacting surfaces is widely used and known as "Lubrication". Basically, the term "lubrication" is associated with the introduction of a fluid film between surfaces that have relative motion, in order to prevent solid contact. Thus, the oil alters solid friction between two solid surfaces to fluid friction, between a solid surface and a fluid. In this paper the lubricant film present in a hydrodynamic bearing was analyzed according to its dynamic characteristics. The evaluation of the coefficients was achieved from the pressure distribution. A finite-difference method was applied to obtain the solution of the Reynolds equation. The coefficients were obtained with a mass-spring-damper concept, in order to represent the inherent flexibility and damping of the oil film. Thus, the feasibility of the application for lubricated bearings with different geometries was evaluated, depending on the rotating speed of the machine, the bearing load and the lubricant viscosity. This procedure allows adjustments for tests at high rotating speeds and high values of applied load.*

Keywords*: Hydrodynamic Lubrication; Multilobe Bearing; Stiffness Coefficients; Damping Coefficients*

1. INTRODUCTION

Journal bearings are, by definition, two elements with relative motion separated by a lubricant fluid, which avoids contact of solid parts and, consequently, wear and failure in rotating machines. The fluid film between moving parts must be able to provide a load capacity with the minimum of energy losses as possible and without introducing undesired instabilities.

Journal Bearings are composed, basically, by a sleeve, with a curved surface (cylindrical, elliptical or multilobe) and a shaft inside, separated from the housing by a fluid film. In the beginning of the motion there is direct contact between the journal (part of the shaft within the bearing) with the sleeve walls. Then the fluid is forced into the region below the journal due to the shear forces generated by the rotation axis. This creates high pressure at the surface shaft. The high pressure supports the weight of the rotor, preventing the journal contact with the surface of the bearing.

The idea of representing the dynamic characteristics of a journal bearing by means of stiffness and damping coefficients was introduced by Stodola (1925) and Hummel (1926). Their aim was to improve the calculation of the critical speed of a rotor by including the flexibility of the bearing oil film. Concurrently, Newkirk (1924 and 1925) described the phenomenon of bearing induced instability, which he called oil whip, and it soon occurred to several investigators that the problem of rotor stability could be related to the properties of the bearing coefficients as can be seen from Castro and Cavalca (2008), Gunter (2005) and Bently (2002).

In the initial stage, one of the difficulties was that the only available solution of Reynolds equation was Sommerfeld's for the infinitely long bearing, sometimes modified by a suitable end-leakage factor, and the only assessments on the rotor dynamics were the calculation of the first critical speed, using the methods of either Rayleigh or Stodola.

In the late forties, more advanced rotor dynamics calculation methods were developed, and with the advent of the computational mechanics in the fifties, it soon became feasible, at little cost, to obtain numerical solutions to the Reynolds' equation and to perform more complete models. Even so, the concept of bearing coefficients was not immediately accepted, probably because the load-displacement characteristic of a journal bearing is so evidently non-linear. Experience, however, has demonstrated the practical utility of the linear coefficients, and the modern rotor dynamics calculations are firmly based on the concept.

The study of dynamic coefficients is a difficult task. Nowadays many efforts have been directed to obtain the problem solution (Meruane and Pascual, 2008; Wang and Khonsari, 2006).

2. THEORY AND RESULTS

2.1 Analysis

In a x - y coordinate system with origin in the bearing center and the x - axis in the static load direction (see Fig. 1), the reaction forces from the lubricant film are given by:

$$\begin{Bmatrix} F_x \\ F_y \end{Bmatrix} = -\int_{-L/2}^{L/2}\int_{\theta_1}^{\theta_2} p. \begin{Bmatrix} \cos\theta \\ \sin\theta \end{Bmatrix} R\, d\theta\, dz \tag{1}$$

where p is the pressure generated within the fluid, R is the journal radius, L is the axial length, z is the axial coordinate and θ is the circumferential angular coordinate from the negative x - axis. The film extends from θ_1 to θ_2 where both angles may be functions of z.

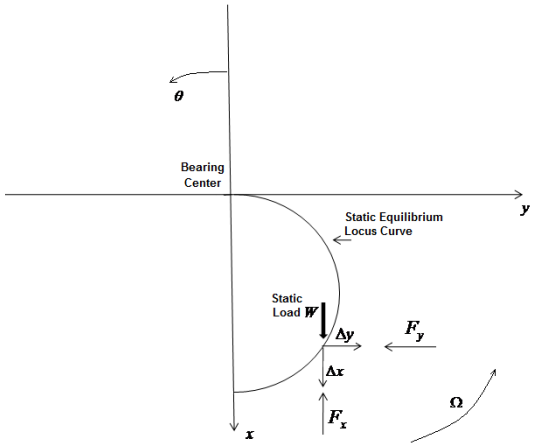

Figure 1. Coordinate system

The basic differential equation, which governs the pressure distribution in the lubricant fluid inside the gap of a journal bearing, is the Reynolds Equation, derived by Osborne Reynolds in his paper in 1886, and it is given by

$$\frac{\partial}{\partial x}\left(h^3\frac{\partial p}{\partial x}\right)+\frac{\partial}{\partial z}\left(h^3\frac{\partial p}{\partial z}\right)=6\mu U\frac{\partial h}{\partial x}+12\mu\frac{\partial h}{\partial t} \tag{2}$$

where t is time, x and z are the Cartesian coordinates, μ is the absolute viscosity of the lubricant, U is the peripherical velocity of the rotor and h is the film thickness, according to the bearing geometry.

$$h = C_r + x\cos\theta + y\sin\theta \tag{3}$$

C_r is the radial clearance, and x - y are the coordinates of the journal center.

The reaction forces are function of x and y, and of the instantaneous journal center velocities, $\dot{x}$ and $\dot{y}$ ("dot" indicates time derivate). Hence, for small deviations, Δx and Δy, measured from the static equilibrium position (x_0 and y_0), a first order Taylor series expansion yields:

$$\begin{aligned} F_x &= F_{x0} + K_{xx}\Delta x + K_{xy}\Delta y + B_{xx}\Delta\dot{x} + B_{xy}\Delta\dot{y} \\ F_y &= F_{y0} + K_{yx}\Delta x + K_{yy}\Delta y + B_{yx}\Delta\dot{x} + B_{yy}\Delta\dot{y} \end{aligned} \tag{4}$$

where the coefficients are the partial derivatives evaluated at the equilibrium position (Lund, 1987):

$$K_{xy} = \left(\frac{\partial F_x}{\partial y}\right)_0 \qquad B_{xy} = \left(\frac{\partial F_x}{\partial \dot{y}}\right)_0 \tag{5}$$

and similary for the remaining coefficients.

At the equilibrium position (x_0, y_0), $F_{y0} = 0$ while F_{x0} equals the static load, W.

In this paper the coefficients are often computed directly by numerical differentiation by employing a perturbation solution. Thus, equation (3) may be written as:

$$h = h_0 + \Delta h \tag{6}$$

where:

$$h_0 = C_r + x\cos\theta + y\sin\theta$$
$$\Delta h = \Delta x\cos\theta + \Delta y\sin\theta \quad (7)$$
$$\frac{\partial h}{\partial t} = \Delta\dot{x}\cos\theta + \Delta\dot{y}\sin\theta$$

Reynolds' Equation is a second-order, non-homogeneous, partial differential equation which is difficult to solve analytically. To solve the equation the finite difference method will be used, with some additional assumptions:

- The viscosity and the density of the lubricant film do not change, maintained a constant load and speed.
- The pressure is assumed zero on the periphery of the journal bearing.

2.2 Finite Difference Method

The Reynolds' Equation was evaluated using a Finite Difference Method (see Pinkus 1956, 1958 and 1959). For this paper, several meshes were tested, and a mesh with 6400 points (80 points in each direction), was the mesh with the best relationship between accuracy and computational cost. Thus, a mesh of 6400 points was chosen and dimensionless pressure on each point of the mesh is given by:

$$p_N = \frac{6\pi\frac{h_L - h_R}{\Delta x} + \left(\frac{D}{L}\right)^2\frac{h_T^3}{\Delta z^2}p_T + \frac{h_R^3}{\Delta x^2}p_R + \left(\frac{D}{L}\right)^2\frac{h_B^3}{\Delta z^2}p_B + \frac{h_L^3}{\Delta x^2}p_L + 12\left(\Delta\dot{x}\cos\theta + \Delta\dot{y}\,sen\,\theta\right)}{\left(\frac{D}{L}\right)^2\frac{h_T^3}{\Delta z^2} + \frac{h_R^3}{\Delta x^2} + \left(\frac{D}{L}\right)^2\frac{h_B^3}{\Delta z^2} + \frac{h_L^3}{\Delta x^2}} \quad (8)$$

Regarding the hydrodynamic forces, the pressure values are integrated numerically in order to provide the vertical and horizontal resultants forces.

$$F_v = \sum_{n=1}^{n} p_N\cos\theta_N(\Delta x)(\Delta z) \quad (9)$$

$$F_H = \sum_{n=1}^{n} p_N\sin\theta_N(\Delta x)(\Delta z) \quad (10)$$

For any given bearing geometry, shaft velocity and load, an equilibrium position of the shaft is given by the boundary condition $F_H = 0$ which can be obtained by assigning the proper value of the eccentricity and the attitude angle.

For the calculation of the bearing dynamic coefficients, the differential form of the Taylor's expansion is evaluated by finite difference.

2.3 Pressure Distribution

The pressure distribution of the oil film inside the bearing is characterized in this section. Analysis are made to a cylindrical bearing, an elliptical bearing and a three-lobe bearing both with pre-load *m=0.5*. The geometric characteristics of each type of bearing is shown in Figure 2.

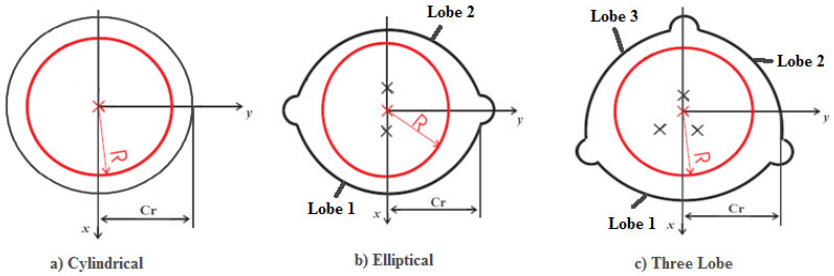

Figure 2. Design of Cylindrical, Elliptical and Three-Lobe Bearings

In all cases, the rotation and applied load are the input parameters and, with the value of these variables and with the geometric data of the bearing, the equilibrium position is found and the pressure distribution is evaluated. The bearing

geometric characteristics and operating parameters are given in Table 1. The lubricant oil is an ISO VG46 at the temperature (T) of 40ºC.

Table 1. Bearing input data

Diameter (m)	Axial Length (m)	Radial Clearance (m)	Load (N)	Viscosity (Pa.s)	Rotation (rpm)
0.18	0.099	1.35×10^{-4}	21384	14.32×10^{-3}	6800

Figures 3 to 8 show the pressure distribution for all the studied cases.

It can be noted (Fig. 5 and Fig.6), for an elliptical bearing, the presence of two peaks of pressure, where 0° to 180° represents the lower lobe of the bearing and 180° to 360°, the upper lobe (Fig. 2b). This can be explained, for this type of bearing, by the fact of for low eccentricity ratios, we have the axis located on the upper semi-plane of the bearing, making the oil film present in the upper lobe to be compressed to generate larger reaction forces and, consequently, a pressure field in that region.

As the tri-lobe bearing is composed by three lobes, it can be notice that its arcs are of 120° (Fig. 2c). The first peak of pressure is related to the lower lobe (1), the central peak corresponds to the right lobe (2) and the last peak, to the left lobe (3). It can be noted by the graphs, Fig. 7 and Fig. 8, the highest pressure is on the lower lobe. The right lobe of the distribution has a slightly higher peak of pressure than the left lobe.

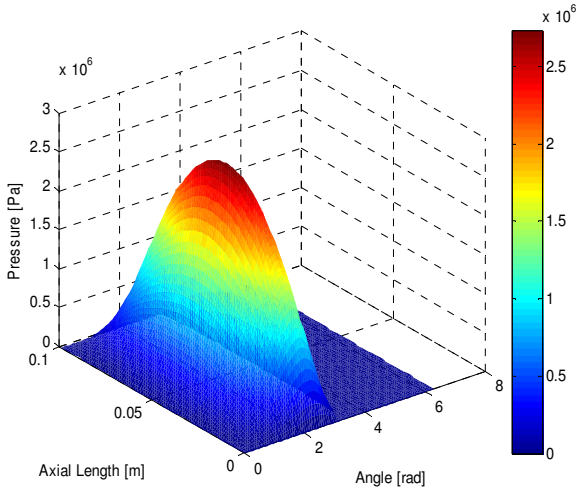

Figure 3: Pressure Distribution Cylindrical Bearing

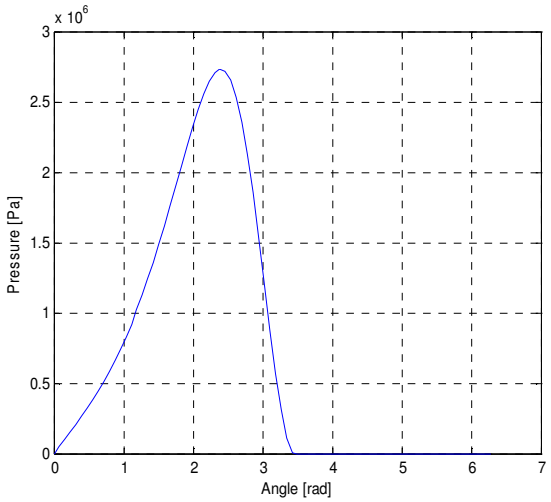

Figure 4: Center Line Pressure Cylindrical Bearing

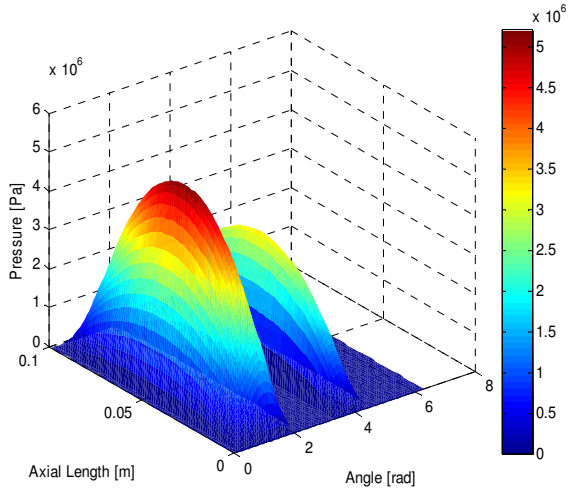

Figure 5: Pressure Distribution Elliptical Bearing

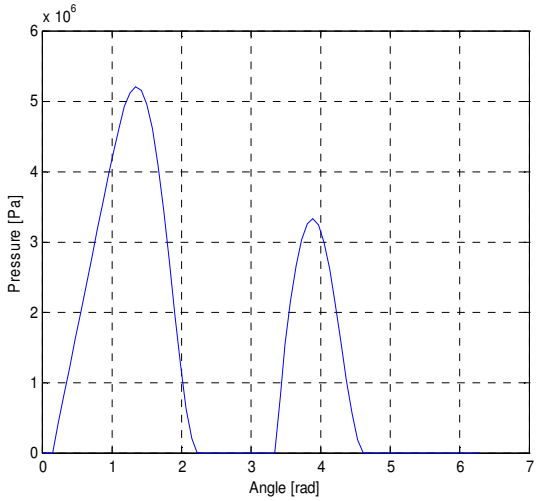

Figure 6: Center Line Pressure Elliptical Bearing

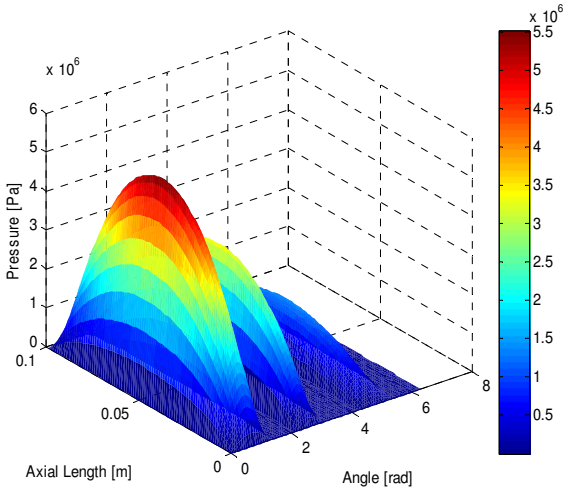

Figure 7: Pressure Distribution Three-Lobe Bearing

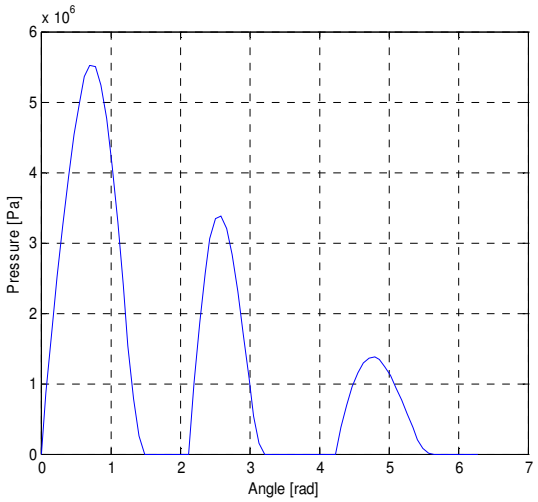

Figure 8: Center Line Pressure Three-Lobe Bearing

2.4 Comparison of Dynamic Coefficients

The results presented in this section were obtained using the numerical model previously described and the geometrical data of a bearing typically used in turbines (Table 1).

This paper provides solutions for three distinct geometries of journal bearings: cylindrical, elliptical and three-lobe. The elliptical bearings had 2 axial grooves of 30-deg arc each and 3 different elliptic ratios (pre-load), *m=0.25, m=0.5* and *m=0.75*. The three-lobe bearings had the same elliptic ratios and no axial grooves.

The following graphics show the stiffness and damping coefficients as a function of the rotation speed for all the different types of bearing used in this paper. The rotation speed was considered at high levels along with high values of applied load as initially proposed.

In all cases, the rotation speed started at 60 rpm (1 Hz) and was increased gradually (1 Hz steps) until the maximum value of 18,000 rpm (300 Hz). In the damping coefficients graphics, the lines that represent the B_{xy} and B_{yx} coefficients were overlapping, and only the red line (corresponding to the B_{xy} coefficient) can be seen. This phenomenon will be discussed later in this paper.

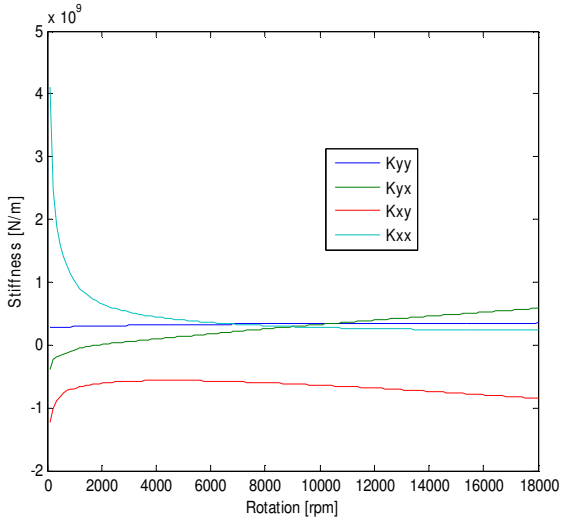

Figure 9: Stiffness Coefficients Cylindrical Bearing

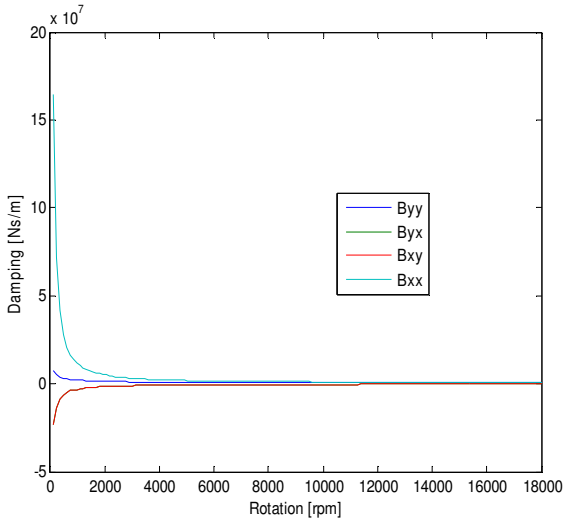

Figure 10: Damping Coefficients Cylindrical Bearing

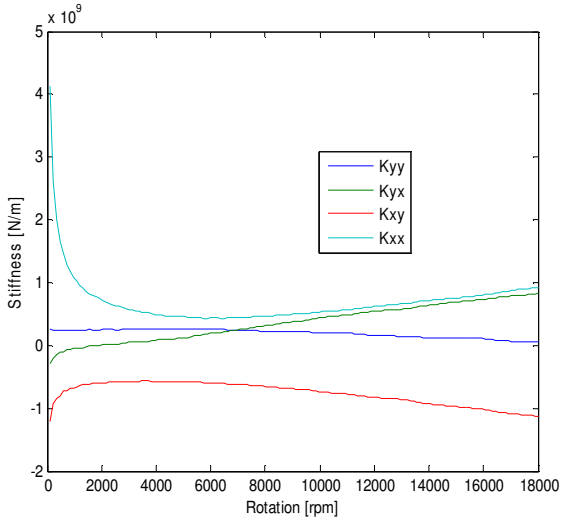

Figure 11: Stiffness Coefficients Elliptical Bearing *m=0.25*

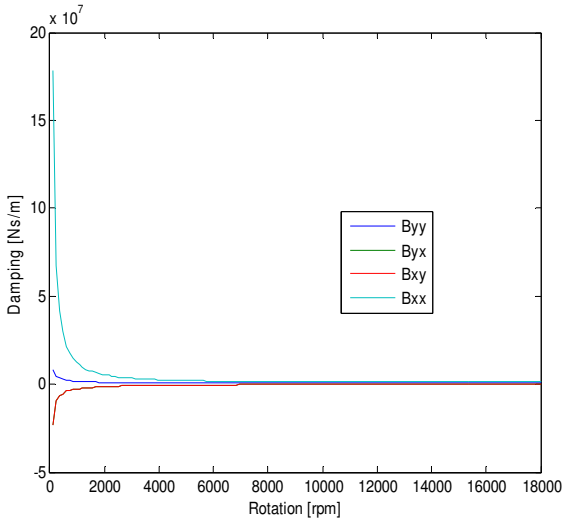

Figure 12: Damping Coefficients Elliptical Bearing *m=0.25*

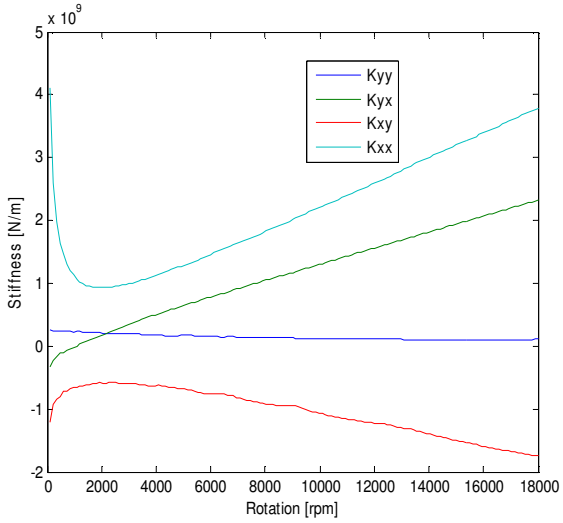

Figure 13: Stiffness Coefficients Elliptical Bearing *m=0.5*

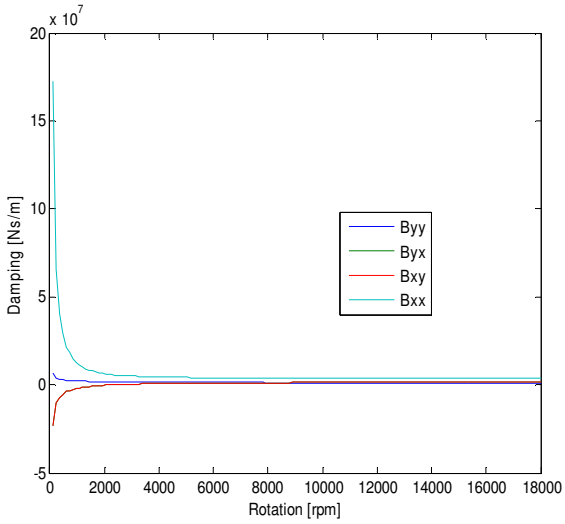

Figure 14: Damping Coefficients Elliptical Bearing *m=0.5*

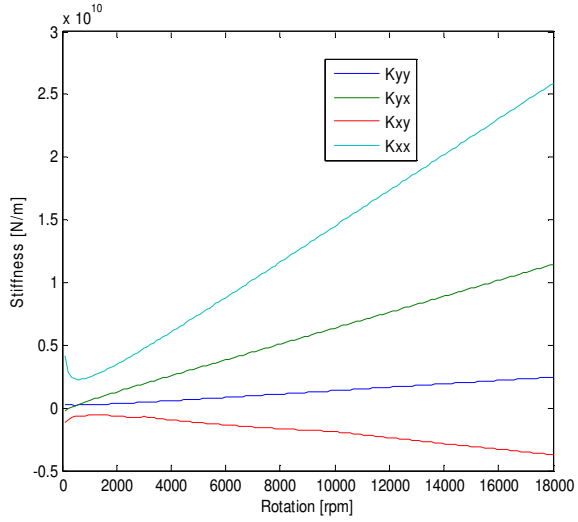

Figure 15: Stiffness Coefficients Elliptical Bearing *m=0.75*

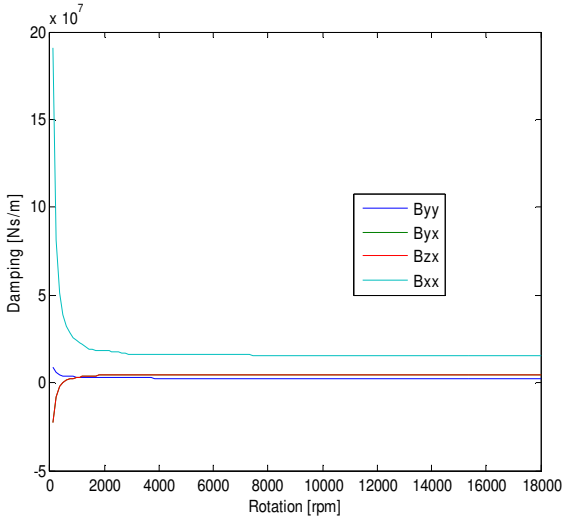

Figure 16: Damping Coefficients Elliptical Bearing m=0.75

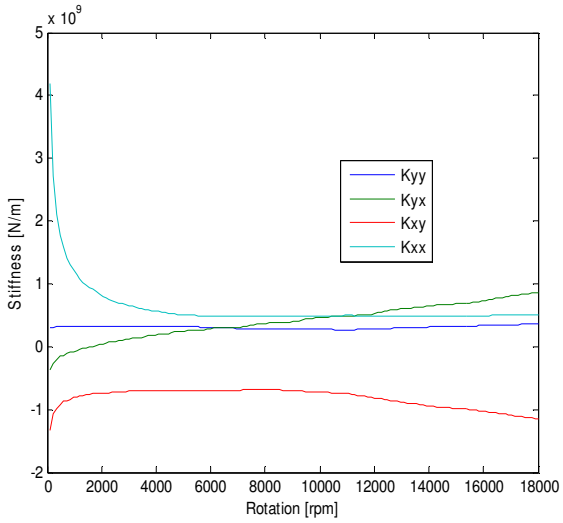

Figure 17: Stiffness Coefficients Three-Lobe Bearing *m=0.25*

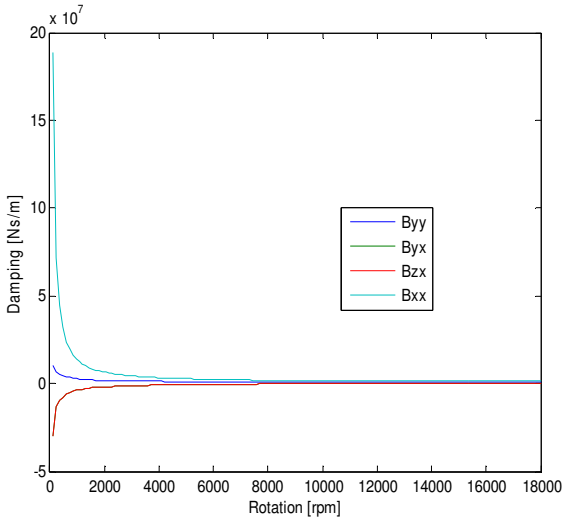

Figure 18: Damping Coefficients Three-Lobe Bearing *m=0.25*

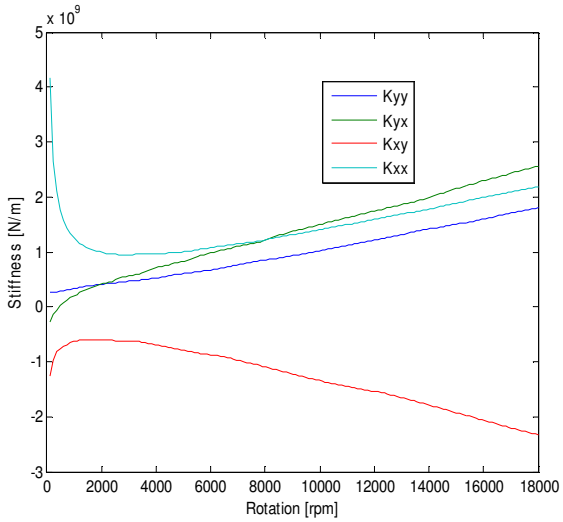

Figure 19: Stiffness Coefficients Three-Lobe Bearing *m=0.5*

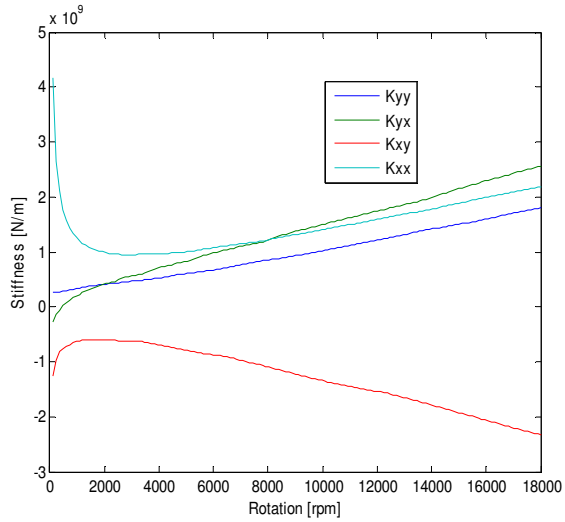

Figure 20: Damping Coefficients Three-Lobe Bearing *m=0.5*

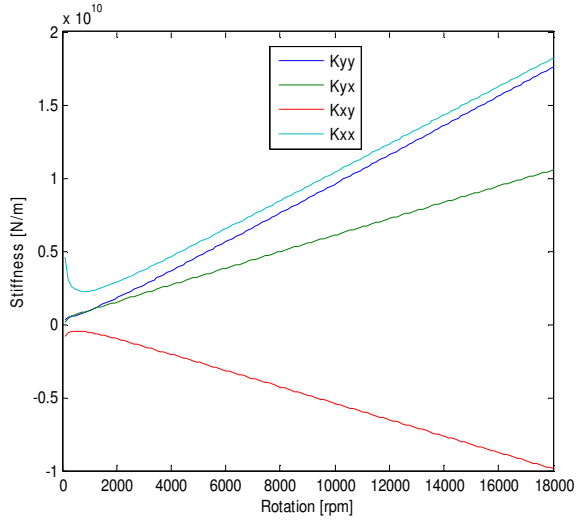

Figure 21: Stiffness Coefficients Three-Lobe Bearing *m=0.75*

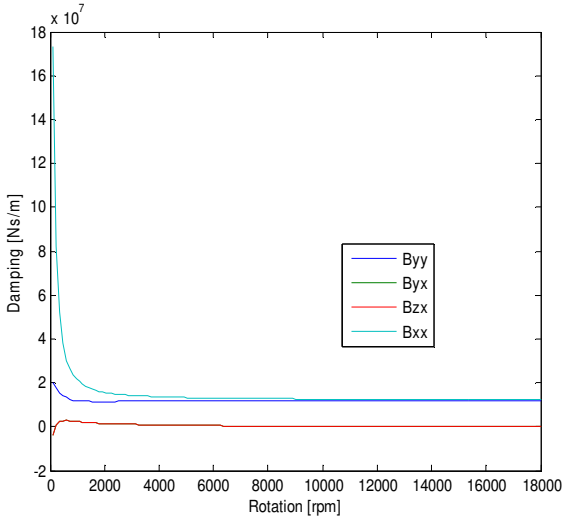

Figure 22: Damping Coefficients Three-Lobe Bearing *m=0.75*

The damping coefficients for all analyzed cases were numerically very close, so were the shape of the curve in the graphics. Regarding the cross-coupling, due to the fact that they derive from self-adjoint operators, these coefficients are coincident. The damping matrix, therefore, will be symmetric and will have principal directions (with an orthonormal basis formed by eigenvectors). That is not true for the stiffness matrix where the cross-coupling stiffness coefficients are unequal, thus the stiffness matrix will be nonconservative (Lund, 1987).

With respect to the stiffness coefficients, it is noted that the values of the cylindrical bearing stiffness is lower than the coefficients of the other two geometries. This is due to the pre-load existing on elliptical and three-lobe bearings. Figures 11, 13 and 15 show a significant increase in the stiffness coefficients on the *x* direction (vertical), in both the cross-coupling and the direct coefficients, for elliptical geometry. That behavior is not observed in the coefficients in the *y* direction (horizontal). This is explained by the fact that the radial clearance used in the cylindrical bearing is the major clearance in the elliptical bearing in the *y* direction (see Fig. 2).

For the three-lobe bearing the stiffness coefficients with low pre-load ($m = 0.25$) are close to the cylindrical bearing. This result comes from the fact that its geometry (3 arcs with 120-deg equally spaced from the bearing center) is closer to a cylindrical bearing. With the pre-load increasing, the stiffness coefficients have a significant increase in magnitude. One can observed that, in addition to the coefficients in the *x* direction (vertical), the direct stiffness coefficient in *y* direction (horizontal) also has a significant increase (Fig. 21).

2.5 Locus of Shaft Center

Figures 23 to 29 show the locus of shaft center for all different types of bearing geometries analyzed. The results are shown in polar-coordinates graphs. The dimensionless eccentricity was evaluated as a function of the attitude angle from an equilibrium position of the shaft. In the elliptical and three-lobe bearings, the values of eccentricity and attitude angle correspond to the total bearing equilibrium position, since these types of bearings have values of eccentricity and attitude angle for each lobe separately.

The eccentricity was evaluated in a dimensionless form related to the radial clearance of the bearing. Hence, when the dimensionless eccentricity is 1, there is metal-metal contact between the shaft and the sleeve, and at a null eccentricity the shaft and the bearing are concentric.

The variation of eccentricity and attitude angle occur with the change in the rotation speed. In all cases there is an increase of the attitude angle and a decrease in the eccentricity with the rotation speed increasing. This is the result of the centralizing tendency of the shaft inside the bearing at high rotation speeds.

Comparing the graphs from Fig. 23 to Fig. 29, it is noticed that for the elliptical bearing, the shaft center often finds itself above the center of the bearing for small pre-loads. This may seem surprising, but a little thought about the dynamics of the oil film will provide the reason. In an elliptical bearing the pressure wedge created in the lower left-hand side has a very high convergence and therefore the resultant horizontal force will be very high. This force is not sufficiently balanced by the forces acting to the lower right-hand side unless the shaft center moves upward and to the right. This movement increases the pressure wedge both on the top half and on the right-hand side of the lower half (see Fig. 5 and Fig. 6).

Regarding the three-lobe bearing, the upper part of the locus curve shows the effect of the two side lobes (see Fig. 7 and Fig. 8), which decrease the curve slope compared to the other bearings slopes. This is very important for the stability of the bearing.

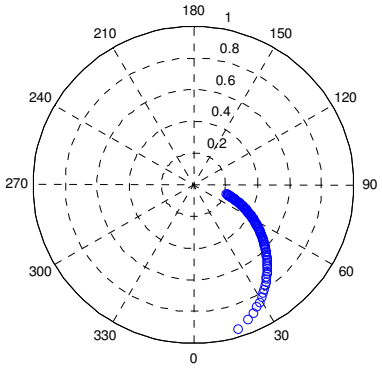

Figure 23: Locus of Shaft Center Cylindrical Bearing

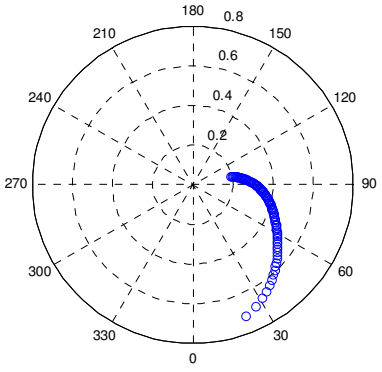

Figure 24: Locus of Shaft Center Elliptical Bearing $m=0.25$

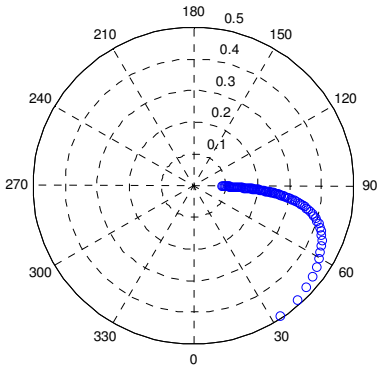

Figure 25: Locus of Shaft Center Elliptical Bearing *m=0.5*

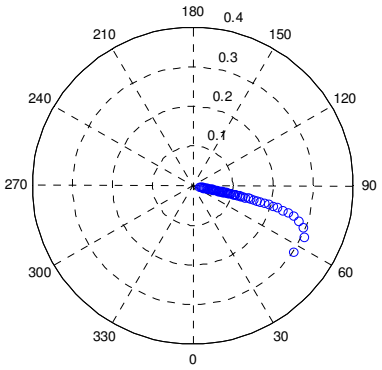

Figure 26: Locus of Shaft Center Elliptical Bearing *m=0.75*

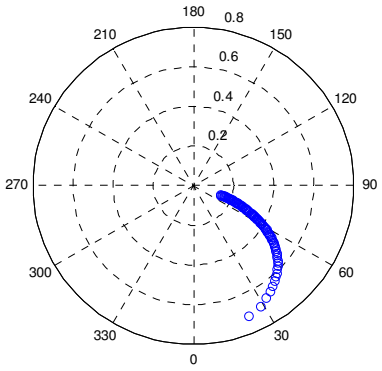

Figure 27: Locus of Shaft Center Three-Lobe Bearing *m=0.25*

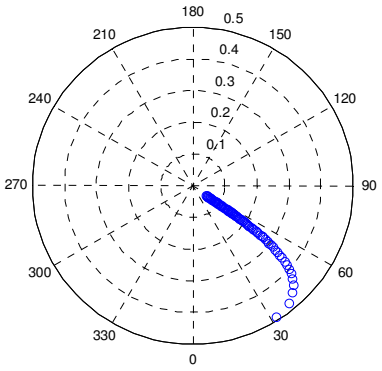

Figure 28: Locus of Shaft Center Three-Lobe Bearing *m=0.5*

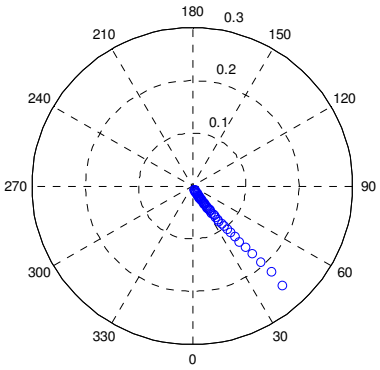

Figure 29: Locus of Shaft Center Three-Lobe Bearing
m=0.75

2.6 General Comments

Results for dynamic coefficients of stiffness and damping are difficult to validate directly due to the paucity of experimental data of these quantities. For the results presented in this paper the validation was made indirectly. The bearing presented in the analysis comes from an industrial application in an energy power plant machine. The frequency

response of all the system is known experimentally, as well as some points in the pressure distribution of the bearing, which indicates the feasibility of the model in the operational frequency range of the system.

Through the analysis of the dynamic coefficients results for different types of bearings, it can be noted that the bearings with pre-load, have an increase in the stiffness coefficients (keeping up the damping coefficients of almost constant) with increasing pre-load. This is due to the fact that as higher the pre-load in the lobes is, smaller is the eccentricity of the bearing and consequently higher is the generate forces in the bearing.

Regarding stability, one can make a qualitative analysis through the relation between the direct and cross-coupling stiffness coefficient. A bearing is usually more stable, at high rotating speed (small eccentricity ratios), as higher is the difference, in module, between the direct and cross-coupling coefficients, in a given direction (Gash at al, 2002). In the cylindrical bearing, for high speeds, direct and cross-coupling coefficients in both directions have the same order of magnitude. In elliptical bearings, with the pre-load increasing, there is a significant increase in the direct stiffness coefficient K_{xx}, for high speeds, making their relative difference (with respect to K_{yx}) larger than in the cylindrical geometry. In the three-lobe bearing, the increase of K_{xx} coefficient is not so expressive as in the case of elliptical bearings, however, its main advantage is that the horizontal direct stiffness coefficient (K_{yy}) also increases, rising the difference between all the cross-coupling and direct coefficients, making the three-lobe bearing one of the most stable fixed geometry bearing.

3. CONCLUSIONS

The finite difference method is proposed to solve the lubrication dynamic model for three different types of journal bearings. The concept of stiffness and damping coefficients for journal bearings has proven very useful, and modern rotor dynamics calculations for unbalance response, damped natural frequencies, and stability are based on this concept. The theoretical limitation of small amplitudes is of little importance in practice, but the analysis still needs improvements, for example as refinements in the model for film rupture. The nonlinear behavior, however, is sometimes of concern in practice, and for practical purposes the instability threshold computed on basis of the linearized coefficients should be adopted as the first approach for the design criterion. As can be also observed, pre-loaded bearings tend to increase stability when at high speeds (small eccentricity ratios). This increase in the stability threshold is due to the fact that each lobe of the bearing has its center of curvature at different points.

4. ACKNOWLEDGEMENTS

The authors thank Schaeffler do Brasil for the financial support of this research, as well as CNPq and FAPESP for research funds.

5. REFERENCES

Bently, D. E., 2002, “Fundamentals of Rotating Machinery Diagnostics”, Bently Pressurized Bearing Press, Minden, NV, USA.

Castro, H. F.; Cavalca, K. L., 2008, “Whirl and whip instabilities in rotor-bearing system considering a nonlinear force model”, Journal of Sound and Vibration, v. 317, pp. 273-293.

Childs D., 1993, “Turbomachinery Rotordynamics”, Wiley-Intersciences, New York, USA.

Gasch, R.; Nordmann R.; Pfützner, H., 2002, “Rotordynamik”, Springer, Berlin, Germany.

Gunter, E. J.; Chen, W. J., 2005, “Introduction to Dynamics of Rotor-Bearing Systems”, Eigen Technologies, Inc, New York, NY, USA.

Hamrock, B. J.; Schmid, S. R.; Jacobson, B. O., 1994, “Fundamentals of Machine Elements”, McGraw Hill, 2nd ed., New York, USA.

Hummel, C., 1926, “Kristische Drehzahlen als folge der Nachgiebigkeit des Schmiermittels im Lager”, VDI-Forschungsheft 287.

Lund, J., 1987, “Review of the Concept of Dynamic Coefficients for Fluid Film Journal Bearings”, ASME Journal of Tribology, vol. 109, pp. 37- 41.

Meruane, V.; Pascual, R., 2008, “Identification of nonlinear dynamic coefficients in plain journal bearings”, Tribology International, v. 41, pp. 743-754.

Muszynska, A., 1988, “Stability of Whirl and Whip in Rotor Bearing System”, Journal of Sound and Vibration, v. 127, pp. 49-64.

Muszinska, A., 2005, “Rotordynamics”. Taylor & Francis Group, Boca Raton, FL, USA.

Newkirk, B. L., 1924, “Shaft Whipping”, General Electric Review, pp. 169.

Newkirk, B. L.; Taylor, H. D., 1925, “Shaft Whipping due to Oil Action in Journal Bearings”, General Electric Review, pp. 559-568.

Pinkus, O., 1956, “ Analysis of Eliptical Bearings”, Trans. ASME, v. 78, pp. 965-973.

Pinkus, O., 1958, " Solution of Reynolds Equation for Finite Journal Bearings", Trans. ASME, v. 80, pp. 858-864.
Pinkus, O., 1959, "Analysis and Characteristics of Three-lobe Bearings", Journal of Basic Engineering, pp. 49-55.
Stodola, A., 1925, "Kristische Wellenstörung infolge der Nachgiebigkeit des Oelpolsters im Lager", Schweizerische Bauzeiting, vol. 85, pp. 265-266.
Wang, J. K.; Khonsari, M. M., 2006, "A new derivation for journal bearing stiffness and damping coefficients in polar coordinates", Journal of Sound and Vibration, v. 290, pp. 500-507.

6. RESPONSIBILITY NOTICE

The authors are the only responsible for the printed material included in this paper.